Volume 2 | Number 17 | 7 May 2014 | Pages 2321–2636

# Journal of Materials Chemistry B

Materials for biology and medicine

www.rsc.org/MaterialsB

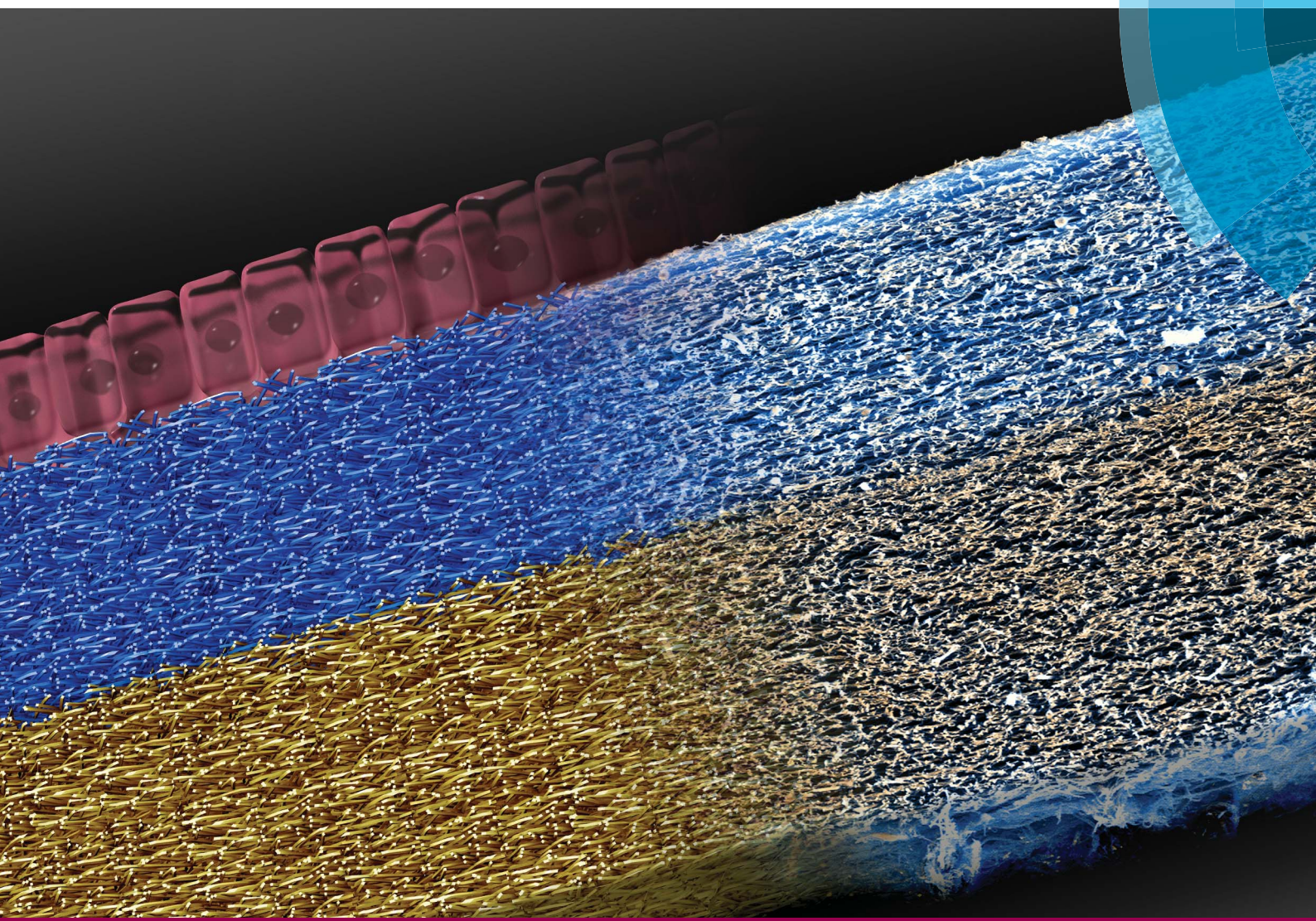

## Themed issue: Emerging Investigators

ISSN 2050-750X

ROYAL SOCIETY OF CHEMISTRY

PAPER

Patricia Y. W. Dankers *et al.*

A modular approach to easily processable supramolecular bilayered scaffolds with tailorable properties

Journal of Materials Chemistry B

PAPER

View Article Online
View Journal | View Issue



Cite this: J. Mater. Chem. B, 2014, 2, 2483

# A modular approach to easily processable supramolecular bilayered scaffolds with tailorable properties†

Björne B. Mollet,[ab] Marta Comellas-Aragonès,[ab] A. J. H. Spiering,[bc] Serge H. M. Söntjens,[d] E. W. Meijer[abc] and Patricia Y. W. Dankers*[ab]

Engineering of anisotropic tissues demands extracellular matrix (ECM) mimicking scaffolds with an asymmetric distribution of functionalities. We here describe a convenient, modular approach based on supramolecular building blocks to form electrospun bilayered scaffolds with tailorable properties. Polymers and peptides functionalized with hydrogen-bonding ureido-pyrimidinone (UPy) moieties can easily be mixed-and-matched to explore new material combinations with optimal properties. These combinatorial supramolecular biomaterials, processed by electrospinning, enable the formation of modular fibrous scaffolds. We demonstrate how UPy-functionalized polymers based on polycaprolactone and poly(ethylene glycol) enable us to unite both cell-adhesive and non-cell adhesive characters into a single electrospun bilayered scaffold. We furthermore show that the non-cell adhesive layer can be bioactivated and made adhesive for kidney epithelial cells by the incorporation of 4 mol% of UPy-modified Arg-Gly-Asp (RGD) peptide in the electrospinning solution. These findings show that the UPy-based supramolecular biomaterial system offers a versatile toolbox to form modular multilayered scaffolds for tissue engineering and regenerative medicine applications such as the formation of membranes for a living bioartificial kidney.

Received 28th October 2013
Accepted 4th February 2014

DOI: 10.1039/c3tb21516d

www.rsc.org/MaterialsB

## Introduction

Most tissues have anisotropic properties, both at structural and functional levels. As a result, tissue engineering often demands anisotropic scaffold materials. This anisotropy can be the result of difference in chemical composition or of physical structure. The simplest form of anisotropy is achieved *via* the formation of a bilayered structure, which results in uniaxial asymmetry. Many examples of bilayered scaffolds are found in the literature in which chemical and/or structural properties vary uniaxially. An example of a single component bilayer is a vascular graft scaffold that is formed from a synthetic, biodegradable elastomer, using two different processing techniques.[1] The inner layer is first produced *via* thermally induced phase separation (TIPS) to form a highly porous sponge structure. Next a microfibrous outer layer is formed directly on top of the inner layer *via* electrospinning. Structural bilayers can also be formed by a single processing technique. For example gelatin and chitosan bilayered scaffolds are formed, with variable pore sizes in each layer *via* a modified freeze-drying procedure.[2] For interface tissue engineering as for osteochondral defects, bilayered scaffolds are needed with tailored space-specific properties, both at biological and mechanical levels.[3] Two separate scaffolds are first produced from different materials with different fabrication techniques, and then joined to form one bilayered scaffold. A bilayer based on anisotropic material composition can easily be formed by the use of one processing technique, as long as layer-by-layer deposition is possible. This has for example been applied in non-woven textile technologies such as electrospinning.[4]

The combination of two or multiple material components is also essential in the development of synthetic biomaterials that can fulfill the role of the extracellular matrix (ECM). Both the development of new materials[5,6] and processing techniques[7,8] have successfully captured parts of the structural characteristics and biological functions of the natural ECM in synthetic materials. However, the complex, multifunctional character of the ECM makes true mimicry an extremely intricate task. In addition, there is a strong tissue related structural variability[9] in these non-static natural scaffolds. The ECM displays ongoing changes upon interaction with cells and overall remodeling plays an important role in for example tissue development and

[a]Laboratory of Chemical Biology, Eindhoven University of Technology, PO Box 513, 5600 MB Eindhoven, The Netherlands. E-mail: p.y.w.dankers@tue.nl; Tel: +31 40 2475451

[b]Institute for Complex Molecular Systems, Eindhoven University of Technology, PO Box 513, 5600 MB Eindhoven, The Netherlands

[c]Laboratory of Macromolecular and Organic Chemistry, Eindhoven University of Technology, PO Box 513, 5600 MB Eindhoven, The Netherlands

[d]SyMO-Chem BV, Den Dolech 2, 5612 AZ Eindhoven, The Netherlands

† Electronic supplementary information (ESI) available. See DOI: 10.1039/c3tb21516d

pathological events.[10,11] Therefore, a material system that allows a modular and/or combinatorial approach will best suffice in finding both optimal and versatile solutions.[12,13]

A relatively new and emerging class of synthetic biomaterials that could fit a modular/combinatorial approach is based on supramolecular interactions. These supramolecular biomaterials are considered to be more natural-like than covalently built-up polymers.[14] Through their reversible, non-covalent bonds these biomaterials are intrinsically able to capture the dynamic character of natural materials and thereby offer additional options to tune the dynamic adaptation of the material on cellular contact. Furthermore, chemical complementarity and structural compatibility can direct multiple weak, non-covalent interactions to participate in stronger, joint interactions leading to molecular self-assembly.[15] This assembly process will not only benefit combinatorial approaches, but also allows for the formation of structurally well-defined materials at the nano-scale as is beautifully exemplified in natural materials.[16] Most examples of synthetic biomaterials that are based on self-assembling/supramolecular interactions form hydrogels or hydrogel-like materials. In general these soft, dynamic materials are considered appropriate materials for potential ECM mimics.[17–19] For several tissue engineering applications, however, a gel-like supramolecular material does not offer the appropriate mechanical properties or structural features required. The engineering of tissues that contain a basement membrane or tough connective tissue, such as for example skin,[20] the bladder,[21] the pelvic floor,[22] or heart valves[23] require a freestanding sheet-like scaffold material with tough or elastic properties. A clear example, by which we exemplify the potential of the supramolecular biomaterial system described in this paper, is the engineering of a bioartificial kidney membrane. The goal of a bioartificial kidney membrane is to keep kidney epithelial cells functional *in vitro* so that their intrinsic capacity to purify blood and to maintain homeostasis, *via* transport, metabolic and endocrine functions, can be utilized to supplement current hemodialysis or hemofiltration treatments.[24,25] In previous approaches kidney epithelial cells were seeded on the coated surface of hollow fibers of commercial filters.[26] These filters are typically made of thermoplastic polymers like polysulfone or polyethersulfone, mixed with a hydrophilic component to prevent adverse adsorption of blood proteins. To allow cell adhesion to one side of these filters, primarily coatings of ECM components have been studied and applied.[27,28] This functional asymmetry is a fundamental requirement of synthetic membranes for the bioengineering of a bioartificial kidney membrane; one hemocompatible and one cytocompatible surface is needed.[29] A bifunctional organization has also been proposed to be an inherent property of the basement membrane, the natural substrate for renal epithelial cells.[30]

Here we focus on a supramolecular material system that allows the capture of the mechanical, hydrophilic and bioactive properties required for the engineering of a bioartificial kidney membrane, by taking advantage of a modular approach. Our supramolecular biomaterial system is based on ureido-pyrimidinone (UPy) units and comprises both UPy-functionalized polymers and UPy-functionalized bioactive peptides. The UPy–moieties are self-complementary *via* fourfold hydrogen bonding, which is a relatively strong but reversible interaction.[31] Hereby, UPy-functionalization of short polymers/oligomers or peptides has the effect of 'molecular Velcro'. In addition, UPy-dimers stack *via* pi–pi interactions that are further aided by adjacent urea linkers.[32] This gives rise to self-assembled nanofibrillar aggregates (see ESI, Fig. SI-1†). These added supramolecular self-assembling interactions can have tremendous effects on the mechanical properties of a polymer, when functionalized with UPy–moieties.[33] We recently showed that supramolecular UPy–polymers can be used as biomaterials. For UPy-end-functionalized polycaprolactone (UPy–PCL), a supramolecular thermoplastic elastomer (TPE), processability with electrospinning was demonstrated. The resulting hierarchical nano- to microfibrous mesh was successfully applied as a 2D cell culture substrate in the field of kidney membrane tissue engineering.[34,35] *Via* modular UPy-functionalization of peptides,[36] facile incorporation of multiple bioactivities into UPy-based polymer biomaterials is achieved[37,38] and the beneficial bioactive effect was demonstrated by improved differentiation of kidney epithelial cells.[35]

In this paper we explore the potential of the UPy-based supramolecular biomaterial system in the formation of modular bilayered scaffolds for a bioartificial kidney membrane. For the first time, we report the use of two different UPy–polymers that are applied in a mix-and-match approach to establish the desired material properties; non-adhesive for cells and suitable mechanical properties to allow the formation of a microfibrous, porous scaffold. Furthermore, this is the first time we show reactivation of cell-adhesion in a non-cell adhesive UPy–polymer mix, by the use of UPy-modified peptides. For this we use UPy-modified variants of two polymers and a bioactive peptide that are frequently used in biomaterials. UPy–PCL is applied as a base component. UPy-modified poly(ethylene glycol) (UPy–PEG) was applied in our modular approach to establish improved wettability and a cell-adhesion resistant character in the scaffold.[39] As a bioactive component the UPy-modified cell-adhesive Arg-Gly-Asp[40] peptide (UPy–RGD) was introduced. The UPy–peptide was adapted from previously reported designs. A short oligo(ethylene glycol) (OEG) linker was inserted between the UPy–moiety and the peptide, to allow presentation of the peptide at the material surface even in the presence of a hydrated PEG-layer and thereby increase availability for interaction with cells. Two bilayered scaffolds were formed *via* layered electrospinning of varying compositions of these three UPy-building blocks (Fig. 1). In the first bilayer, UPy–PCL and UPy–PEG were applied in a mix-and-match approach to generate a cell-adhesive layer and a non-cell adhesive layer. The second bilayer was entirely based on the non-cell adhesive material mixture, but one side was supplemented with a small quantity of UPy–RGD to stimulate cell adhesion. Both scaffolds were investigated for chemical composition, morphology and hydrophilicity at their surfaces, and their effect on adhesion ability and morphology of human kidney epithelial cells. In addition, more detailed cell-studies were performed on thin electrospun meshes and

 

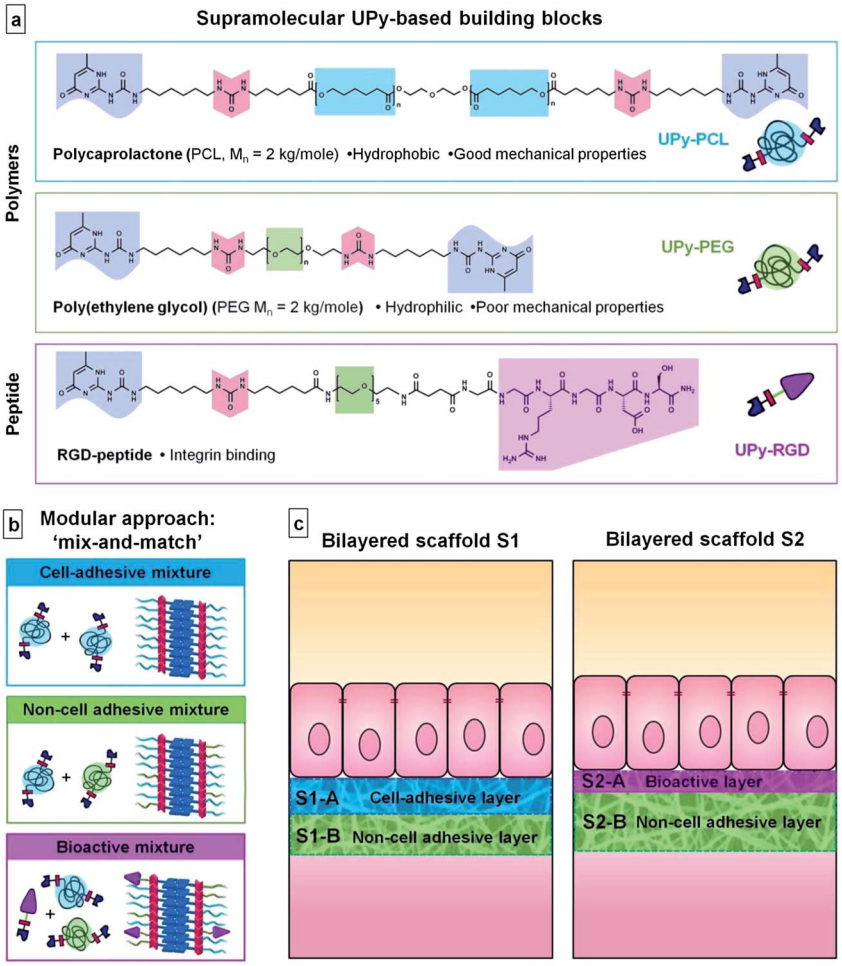


Fig. 1 (a) Chemical structures and schematic representations of the supramolecular polymers UPy–PCL and UPy–PEG and the supramolecular bioactive component, UPy–RGD. (b) Schematic representations that show the proposed incorporation of the different UPy-building blocks into stacks of UPy-dimers when mixed, and (c) bilayered scaffolds S1 and S2 that are electrospun using these combined supramolecular building blocks. These bilayered scaffolds are designed to facilitate cell adhesion on their top layer A and to prevent cell adhesion to the bottom layer B.

dropcast films of the three UPy–biomaterial mixtures. To our knowledge, this is the first example where PCL, PEG and RGD are employed in a supramolecular material system that can be used in a modular approach by single-step electrospinning to form freestanding biomaterial scaffolds.

## Materials and methods

### Synthesis of UPy–polymers and UPy–peptide

The syntheses of the compounds UPy–PCL,[41,35] UPy–PEG and UPy–RGD peptide[42,36] are described in the ESI.† The synthesis of UPy–PCL was adapted from previously described approaches but performed in a more scalable manner using different protection group chemistries.

### Preparation of electrospun bilayered scaffolds and thin meshes on glass

**Bilayered scaffold S1.** Two electrospinning solutions were prepared in glass vials. For the bottom layer (S1-B) 17.5 wt/wt% UPy–PCL was dissolved in 82.5 wt/wt% 1,1,1,3,3,3-hexafluoro-2-propanol (HFIP, 147545000, Acros) (B). For the top layer (S1-A), 7.5 wt/wt% UPy–PEG was first dissolved in 75 wt/wt% HFIP, then 17.5 wt/wt% UPy–PCL was added (A). The solutions were stirred overnight at room temperature and then transferred to separate 2.5 mL glass syringes (Hamilton). Approximately 1 mL of the first solution (B) was fed at 0.02 mL $min^{-1}$ using a syringe pump (KR analytical) at the outside of the electrospinning cabinet to the flat-tip stainless-steel 23 g needle (Intertronics, United Kingdom) inside the cabinet, *via* a 35 cm long 1 mm I.D. PTFE tube. Inside the cabinet, the solution was spun with an in-house built electrospun setup by the application of 18.5 kV between a tip-to-target distance of 12 cm. Fibers were collected on a 12 × 12 cm grounded collector plate. To enable facile removal of the non-woven electrospun membrane, the collector was covered with a thin sheet of polyethylene film. The fiber deposition was interrupted several times to move the static collector plate over a 3 × 3 grid to enlarge the area of fiber deposition and to achieve a more homogeneous layer thickness. Then the feeding syringe was replaced with the syringe

containing mixed polymer solution A and the flow rate was set at 0.015 mL $min^{-1}$. Small indentations were created along the thin edges of the electrospun layer S1-B to enable visual control of evenly distributed fiber deposition during spinning of the second layer S1-A. Fibers, again formed from approximately 1 mL polymer solution, were collected on top of the previously deposited fiber layer S1-B. The polyethylene film was gently removed from the electrospun scaffold. The scaffold was placed *in vacuo* at 40 °C overnight to remove any residual solvent.

**Bilayered scaffold S2.** The electrospinning solution for bottom layer S2-B was prepared as for bilayered scaffold S1, by first dissolving 7.5 wt/wt% UPy–PEG in 75 wt/wt% HFIP, after which 17.5 wt/wt% UPy–PCL was added. For the top layer (S2-A) first 4 mol% UPy–RGD (compared to total mol polymer) was dissolved in the appropriate amount of HFIP (75 wt/wt%), then 7.5 wt/wt% UPy–PEG was added to dissolve and last 17.5 wt/wt% UPy–PCL. Electrospinning was performed as described for bilayer S1.

**Thin meshes on glass.** For meshes on glass, three polymer solutions, UPy–PCL, UPy–PCL+ 30 wt% UPy–PEG and UPy–PCL+ 30 wt% UPy–PEG + 4 mol% UPy–RGD, were prepared as for the bilayered scaffolds. Also equal electrospinning settings were applied. On top of the collector plate, which was covered with a thin sheet of polyethylene (PE) film, round glass coverslips of 12 mm Ø were placed. Electrospun fibers were collected until an opaque, thin sheet was formed. The glasses with meshes were removed from the collector together with the PE film and placed as a whole *in vacuo* at 40 °C overnight to remove any residual solvent.

### Preparation of dropcast films on glass coverslips

The UPy–biomaterial solutions as used for the preparation of electrospun meshes on glass were diluted five times in HFIP. Thin dropcast films were prepared by distributing 25 μL of such a solution on a 12 mm Ø glass coverslip. The HFIP was evaporated. To remove any residual solvent, the dropcast films on glasses were placed *in vacuo* at 40 °C overnight.

### Characterization of electrospun bilayered scaffolds and thin meshes on glass

**Scaffold morphology: scanning electron microscopy.** Environmental scanning electron microscopy (ESEM) imaging was performed by using FEI Quanta 600 and Xt Microscope Control software. Samples were prepared by placing small pieces of each scaffold, facing top and bottom side up, and a sample of each batch of meshes on glass, on double-sided sticky carbon tape on a metal stub. A cross-section of the scaffolds was gently cut with a razor blade and placed sideways on the tape. The uncoated samples were directly visualized in a low vacuum (~0.5 mbar) with an accelerating voltage of 18 kV and a working distance of 8 mm. Images were recorded up to 10 000 times magnification. Both backscattering electrons (BSEs) and secondary electrons (SEs) were detected. Artificially colored images were constructed by overlaying the resulting images from both detectors. Microfiber diameters were determined from multiple high magnification images using ImageJ software and expressed as average ± standard deviation.

**Chemical composition of bilayered scaffold surfaces: infrared spectroscopy.** Infrared spectra were recorded on a Fourier transform infrared spectrometer (Perkin Elmer Spectrum Two, with a Universal ATR sampling Accessory and diamond crystal, Perkin Elmer Instruments, The Netherlands). Transmission spectra were recorded at room temperature in the range of 4000–450 $cm^{-1}$ at a resolution of 4 $cm^{-1}$ and with an accumulation of 4 scans. Both sides of the bilayered scaffolds were measured separately. A sample was placed on the crystal and covered with a glass slide. Then gentle force was applied on top of the glass slide using a flat shoe to achieve good contact between the sample and the crystal. As control, spectra of both pure UPy–PCL and UPy–PEG were recorded. Transmission spectra were normalized to the maximum intensity peak (1728 $cm^{-1}$, C=O stretch vibrations of the ester carbonyl group for UPy–PCL containing samples and 1094 $cm^{-1}$, ether C–O–C stretch in pure UPy–PEG).

**Hydrophilicity of bilayered scaffolds: water contact angle measurements.** Water contact angle measurements were performed on a contact angle system OCA 30 from Dataphysics using SCA20 software. Round-shaped 0.5 cm Ø samples were cut from the bilayered scaffolds and fixed on a glass microscopy slide using double sided sticky-tape. For each scaffold side, three samples were prepared and measured. A 50 μL drop of deionized water was placed in the middle of each sample and images were captured at a rate of 25 frames per second, up to 60 seconds after placement of the water drop. Water contact angles were determined from the recorded images. The mean of three samples ± standard deviation was expressed.

### Cellular response to UPy–biomaterials: human kidney-2 cell adhesion and cell morphology

**Human kidney-2 cell culture.** Human kidney-2 (HK-2) cells, an immortalized proximal tubule epithelial cell line,[43] were routinely cultured on tissue culture treated polystyrene in complete medium consisting of Dulbecco's Modified Eagle Medium (DMEM, Gibco) supplemented with 10 v% heat inactivated fetal bovine serum (26140-079, Gibco, Invitrogen) and 1 v% penicillin–streptomycin solution (Gibco, Invitrogen), at 37 °C and 5% $CO_2$ in a humidified atmosphere. Cells, cultured up to 80–90% confluence in a T75 flask (BD Falcon), were washed with phosphate buffered saline (PBS, Sigma Aldrich) twice and detached from the culture flask using 0.05% trypsin–EDTA (25300-054, Gibco, Invitrogen). Trypsin was inactivated by addition of complete medium. The cell suspension was transferred to a 50 mL falcon tube and centrifuged at 300 *g* for 5 minutes. The supernatant was aspirated and the cell pellet was resuspended in a known volume of complete medium. Cell concentration was determined *via* cell counting in a hemocytometer.

**UPy–biomaterial sample preparation and cell seeding.** Round-shaped 12 mm Ø samples were cut from the bilayered scaffolds. For the meshes, individual 12 mm Ø glasses covered with a UPy–biomaterial mesh were separated from the PE sheet.

 

Samples were sterilized *via* UV-irradiation for 1 hour on each side. Samples were fixed in MINUSHEET tissue carriers with 13 mm O.D. (Minucells and Minutissue vertriebs gmbh). For each bilayered scaffold different samples had either side A or side B facing up. The carriers with samples were placed in a 24-well tissue culture plate (BD Biosciences). Each bilayered scaffold sample was wet in an ample volume of complete medium, which was removed right before cell seeding until the fluid level reached the upper surface of the carrier, followed by removal of residual medium on top of the scaffold sample.

After cell trypsinisation, the concentration of the cell suspension was adjusted. On each scaffold sample $180 \times 10^3$ HK-2 cells were seeded in 50 μL within the opening of the carrier ring. For the meshes and films on glass two densities were seeded, $36 \times 10^3$ (low) or $180 \times 10^3$ (high) in 75 μL within the opening of the carrier ring on the dry samples. In all cases the cells were initially left to adhere for 2 hours at 37 °C, 5% $CO_2$ and 90% humidity, then 700 μL of complete medium was added per well and cells were further cultured for 12 hours or 3 days.

**Cell fixation, staining and visualization**

*Bilayered scaffold samples.* After the culture period, the scaffold samples were washed with PBS twice. Then adhered cells were fixed by incubation with 4 v% formaldehyde (Fluka) in PBS solution for 10 minutes at room temperature. Samples were again washed with PBS twice and subsequently incubated for 1 hour with blocking buffer of 5 wt/v% BSA (Sigma Aldrich) in PBS. The cell's actin skeleton was stained with atto-488-conjugated phalloidin (1 : 1000, Sigma Aldrich) in 2 wt/v% BSA in PBS by incubation at room temperature for 60 minutes, then cell nuclei were stained with Hoechst (1 : 1000, Sigma Aldrich) for 15 minutes. The samples were washed three times with PBS, taken out of the supporting rings and embedded between a microscopy slide and cover glass in Vectashield (Brunschwig Chemie). The samples were visualized by fluorescence microscopy using a 20× magnifying objective on a Zeiss Axio observer D1 equipped with an AxioCam Mrm camera and Zeiss Axiovision software (Carl Zeiss).

*Meshes and films on glasses.* After the culture period, the samples were washed with PBS twice. Then adhered cells were fixed by incubation with 4 v% formaldehyde (Fluka) in PBS solution for 10 minutes at room temperature. Samples were again washed with PBS twice and subsequently cells were permeabilized by incubation with 0.5 v/v% Triton X-100 (Sigma Aldrich) in PBS for 10 minutes at room temperature. The samples were washed with PBS twice before incubation for 1 hour with blocking buffer of 5 wt/v% BSA (Sigma Aldrich) in PBS.

Samples fixed at 14 h after cell seeding were stained for actin, vinculin and nuclei. First samples were incubated for 1 hour with mouse anti-human vinculin (1 : 400, Sigma Aldrich) in 2 wt/v% BSA in PBS, followed by washing with 0.1 v/v% polysorbate 20 (Merck) in PBS twice and PBS once. Then samples were incubated for 45 minutes with goat anti-mouse Alexa 555 conjugated antibody (1 : 400, Molecular probes, Invitrogen) and atto-488-conjugated phalloidin (1 : 500, Sigma Aldrich) together with 2 wt/v% BSA in PBS, directly followed by incubation for 10 minutes with 4′,6-diamidino-2-phenylindole (DAPI, 1 : 1000, Invitrogen) in 2 wt/v% BSA in PBS. The samples were washed with 0.1 v/v% polysorbate 20 in PBS twice and once in PBS.

Samples fixed 3 days after cell seeding were stained for zona occludens-1 (ZO-1), vinculin and nuclei. The staining protocol is as described for the samples fixed at 14 h after cell seeding, except for the first antibody incubation step, mouse-anti-human ZO-1 (1 : 100, BD Biosciences) was used.

After staining, samples were taken out of the supporting rings, if possible the supporting glass coverslip was removed, and the mesh or film was embedded between a microscopy slide and cover glass in glycerol–PBS solution (Citifluor, Agar scientific). The samples were visualized by fluorescence microscopy using a 10× and 20×, and 40× oil magnifying objective on a Zeiss Axio observer D1 equipped with an AxioCam Mrm camera and Zeiss Axiovision software (Carl Zeiss).

## Results and discussion

### Preparation and morphology of bilayered electrospun scaffolds

Two different bilayered scaffolds, S1 and S2, with distinct layer properties were prepared *via* layered electrospinning. The first bilayer (S1) aimed to include a layer adhesive for cells *via* aspecific interactions (S1-A), and one non-cell adhesive layer (S1-B). In the second bilayer (S2) the non-cell adhesive layer (S2-B) was combined with a layer (S2-A) that is adhesive for cells, only *via* specific interactions. The relatively hydrophobic UPy–PCL was applied to form the cell-adhesion compatible layer S1-A. In layer S1-B 30 wt% of the hydrophilic UPy–PEG was added in the electrospinning process, with the aim to form a non-cell adhesive layer. This change in electrospin composition was achieved by simply exchanging the feeding syringe attached to the PTFE tubing that guided the solution to the spinning needle, for another feeding syringe that had been pre-filled with the new solution of UPy–polymers. In this layer UPy–PCL and UPy–PEG were mixed, since UPy–PEG alone could not be processed into a fibrous polymer mesh using electrospinning (ESI, Fig. SI-2†). The addition of 30 wt% UPy–PEG to UPy–PCL did not negatively influence the electrospinning process at the chosen processing settings. SEM imaging was performed in low vacuum mode without the application of a conducting layer, such as sputtered gold, on the specimen. This allowed recording of both backscattering electron (BSE) and secondary electron (SE) signals directly from the sample and hence the ability to distinguish between both layers based on a small difference in chemical composition (Fig. 2). The layers are tightly adhered as shown by the absence of a sharp transition at their interface. It was found that the layers formed one continuous membrane when the electrospinning solution was fed continuously. The fiber density throughout bilayer S1 was evenly distributed, as observed in a cross-section of the scaffold. The top and bottom-views of bilayer S1 showed similar morphologies (Fig. 2). The deposition of randomly oriented fibers with diameters typically in the submicron range resulted in apparent pore sizes smaller than 5 μm for both layers S1-A and S1-B (top and bottom views), which should allow adherent

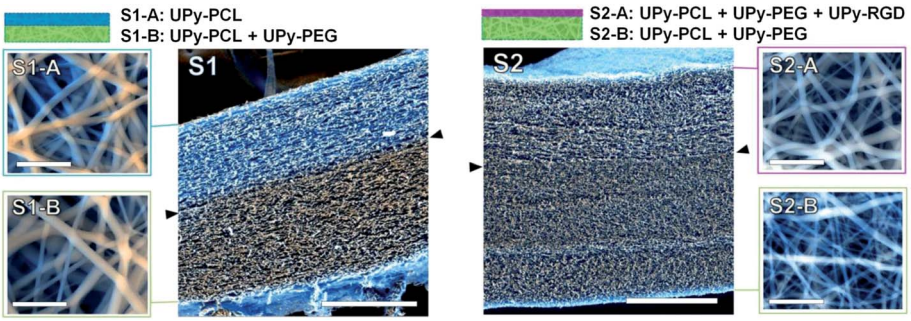


Fig. 2 SEM micrographs of electrospun bilayered scaffolds S1 and S2. In the cross-section of the scaffolds the layer transition is indicated by the arrows (scale bars represent 200 μm). Top and bottom views show the fiber diameters and apparent pore sizes of each scaffold layer (scale bars represent 5 μm). Average fiber diameters ± standard deviation were determined from these and other images: S1-A: 576 ± 215 nm, S1-B: 636 ± 359 nm, S2-A: 428 ± 226 nm, S2-B: 283 ± 139 nm.

cells to grow on top of the scaffold surface, rather than inside the scaffold.

In bilayered scaffold S2, both layers S2-A and S2-B were formed using the supramolecular polymer combination of UPy–PCL + 30 wt% UPy–PEG, with 4 mol% of cell-adhesive UPy–RGD added to layer S2-A. Hence, the difference in atomic composition between the layers of scaffold S2 was very small and was not observed in SEM imaging. For scaffold S2, the transition between both layers in the cross-section was marked by a slightly more densely packed fiber structure in layer S2-B. This correlated with the overall smaller fiber diameter (283 ± 139 nm) in this layer as observed in the bottom-view of the scaffold, compared to layer S2-A in the top-view of the scaffold (428 ± 226 nm).

Successful electrospinning of the layered scaffolds demonstrates that the UPy-based biomaterial approach allows the facile combination of different UPy–polymers and UPy–peptide to construct layered scaffolds with this processing technique. Furthermore, successful electrospinning of layers S1-B and S2-B demonstrates that a convenient combination of different UPy–polymers into new supramolecular copolymers is possible *via* a mix-and-match approach. This allows us to make use of distinct polymer properties in a joint supramolecular biomaterial assembly, and thereby allows tailoring of scaffolds towards desired requirements.

## Chemical composition and wettability of bilayered scaffold surfaces

FTIR spectroscopy was performed on both the top and bottom layers of scaffolds S1 and S2. The recorded spectra were compared to reference spectra of pure UPy–PCL and UPy–PEG to monitor the chemical composition of each layer surface (Fig. 3). As expected the spectrum of layer S1-A corresponded to pure UPy–PCL. For layer S1-B, a mixed spectrum of UPy–PCL and UPy–PEG was observed. This was especially seen in the changed ratio of C–O vibrations at 1160 $cm^{-1}$ (ester) and 1094 $cm^{-1}$ (ether). This indicated that both UPy–PEG and UPy–PCL were present at the surface of the electrospun fibers. For bilayered scaffold S2 the spectra of both layers S2-A and S2-B corresponded, as expected, to this mixed polymer composition.

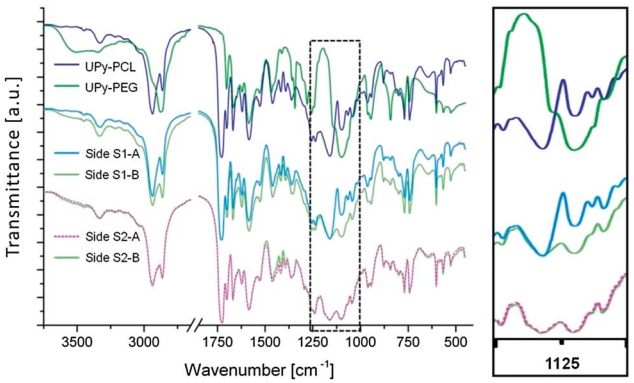


Fig. 3 FTIR analysis of pure UPy–PCL, UPy–PEG, and of both sides A and B of the electrospun bilayered scaffolds S1 and S2: (S1-A) UPy–PCL, (S1-B, S2-B) UPy–PCL + 30 wt% UPy–PEG and (S2-A) UPy–PCL + 30 wt% UPy–PEG + 4 mol% UPy–RGD. The marked and enlarged region indicates the most pronounced change in the FTIR spectra when mixing UPy–PEG and UPy–PCL.

The presence of UPy–RGD in layer S2-A was not observed by this technique. This does not mean that the RGD peptide was not present at the surface of scaffold layer S2-A. The UPy–RGD largely resembles the UPy–PEG and UPy–PCL in terms of chemical bond composition. Only the peptide part would generate distinct signals in FTIR. However, this technique was not sensitive enough to detect the small quantity of UPy–RGD that was added.

Water contact angle (WCA) measurements were performed to study the influence of UPy–PEG on the wettability of the electrospun layers (Table 1). Images were recorded at a rate of 25 frames per second, up to 60 seconds after an initial contact. Layer S1-A, composed of 100% UPy–PCL, showed high contact angles (120.5 ± 2.5°). This was as expected for the hydrophobic PCL backbone in this supramolecular polymer and the additional reducing effect on the wettability by the roughness of the electrospun fibrous morphology.[44] Furthermore, no significant decrease of contact angle was observed during the measuring period of 60 seconds. Also, the drop did not change in size, indicating that water was not able to enter the pores of the scaffold within the timeframe measured. So this material did

 

Table 1 Water contact angles (°) are high and stable for 60 seconds on porous electrospun UPy–PCL (S1-A). In the presence of 30 wt% UPy–PEG (S1-B, S2-B, S2-A) contact angles are reduced by ≥50% and water is quickly absorbed by the porous membrane; within 2 seconds no visible drop was left to determine contact angles

| | S1-A | S1-B | S2-B | S2-A |
|---|---|---|---|---|
| Time (s) | UPy–PCL | UPy–PCL + UPy–PEG | UPy–PCL + UPy–PEG | UPy–PCL + UPy–PEG + UPy–RGD |
| 0.0 | 120.5 ± 2.5 | 50.0 ± 2.9 | 60.1 ± 4.0 | 55.5 ± 4.4 |
| 0.2 | — | 40.1 ± 6.0 | 47.0 ± 5.2 | 35.0 ± 9.1 |
| 0.4 | — | 31.7 ± 5.1 | 39.6 ± 6.2 | 21.2 ± 15.2 |
| 1.0 | — | 17.7 ± 8.8 | 18.0 ± 1.4 | 15.7 ± 7.3 |
| 2.0 | — | NA | NA | NA |
| 10.0 | 120.0 ± 2.4 | — | — | — |
| 60.0 | 119.4 ± 2.7 | — | — | — |

not easily wet. A completely different behavior was seen for scaffold layer S1-B in which hydrophilic UPy–PEG was present. Upon initial contact with the scaffold the water contact angle was 50.0 ± 2.9°, which was significantly lower compared to S1-A. This indicated that the surface of S1-B was more hydrophilic than the surface of S1-A, and that this was caused by the addition of 30 wt% UPy-PEG during the electrospinning of layer S1-B. After initial contact, the angle quickly reduced further. This was attributed to the absorbance of water into the porous material. As the volume of the drop on top of the scaffold reduced, the height of the drop reduced and hence the contact angle became smaller until it could no longer be measured. This state was reached within 2 seconds. For bilayer S2, the observed initial contact angles for sides S2-A and S2-B were 55.5 ± 4.4° and 60.1 ± 4.0°, respectively. For both sides similar quick drop absorption times (<2 s) were observed. Although the chemical compositions of layers S1-B and S2-B were equal, a difference in the average initial contact angle of ~10° was observed. This could be attributed to the minor morphological difference; water had more difficulty to penetrate the slightly smaller apparent pores of S2-B. However, the limited speed at which the images were recorded (25 frames per s), combined with the fast absorption of water, caused an offset in what we observed as the initial contact; for some samples a decrease of >10° was observed between two consecutive frames directly after the initial contact.

The FTIR results show the presence of UPy–PEG at the surface of layers S1-B, S2-B and S2-A. According to WCA measurements, this leads to an increase of hydrophilicity and extreme enhancement of scaffold wettability. Bilayered scaffold S1 demonstrates a uniform structure while anisotropic chemical composition results in distinct wettability of each scaffold side. This uniaxial asymmetry is a result of the layered processing technique. There are no indications of demixing of the building blocks within each layer. The small confinement of the different components during the formation of electrospun fibers and the fast evaporation of the single solvent may contribute to a homogeneously mixed distribution of components, but the shared UPy-functionality is assumed to further enhance the establishment of a molecularly mixed composition *via* the formation of a joint supramolecular biomaterial assembly.

### Cell adhesion and cell morphology on bilayered scaffolds

Human kidney epithelial cells (HK-2) were seeded in a high density ($180 \times 10^3$ cells per sample) on the bilayered scaffolds to investigate the effect of increased hydrophilicity and introduced bioactivity in the separate scaffold layers. Cell adhesion and morphology was studied 14 hours after cell seeding by visualizing the actin cytoskeleton using fluorescently labelled phalloidin (Fig. 4, nucleic stain is shown in the ESI, Fig. SI-3†). For bilayered scaffold S1, cell adhesion and spreading on layer S1-A confirmed the cell-adhesive character of electrospun UPy–PCL as observed in previous studies.[34,35] The addition of 30 wt% UPy–PEG to layer S1-B, which showed increased hydrophilicity and scaffold wettability, was hypothesized to reduce cell adhesion. Indeed fewer cells were observed on layer S1-B. In addition these cells remained in a rounded morphology, indicating that no cell spreading or proper cell adhesion occurred. Similar lowered cell density and round morphology was observed for scaffold S2 on layer S2-B. In contrast, different cell behavior was observed for the HK-2 cells that were seeded on scaffold layer S2-A. Here HK-2 cells adhered, spread and formed a near confluent cell layer. The chemical difference of layer S2-A compared to both layers B of scaffolds S1 and S2 was only 4 mol % UPy–RGD. This demonstrated that at least part of the RGD-peptide that was mixed with the electrospinning solution was presented at the surface of the polymer fibers, available for specific interaction with cells. This has not been demonstrated for a two-component UPy–polymer mix before. Here the presence of the hydrophilic UPy–PEG component might interfere with the surface presentation of the peptide, in particular when the material is hydrated in the aqueous cell culture environment. To anticipate this effect, a short oligo(ethylene glycol) linker was incorporated between the UPy–moiety and the peptide to allow bridging of the expected hydrated PEG-layer at the material surface. The difference in cell behavior between layer S2-A and both layers B did not only confirm RGD-peptide presentation at the surface, but also shows that the amount of peptide present at the surface provided enough anchoring points to allow the HK-2 cells to adhere and spread on an otherwise cell-adhesion repulsive material. Nonetheless, the applied quantity of UPy–RGD might still be optimized. Possibly smaller amounts of bioactive compounds provide equal or even better effects with respect to cell adhesion. For HK-2 cells cultured on electrospun fibrous substrates consisting of polymethylmethacrylate (PMMA) with different collagen I coatings, it has been reported that the largest amount of proteins adsorbed on fibers does not lead to the best performance in terms of cell attachment and proliferation *in vitro*.[45]

### Detailed investigation and discussion of the interaction between HK-2 cells and UPy-biomaterials

The interaction between cells and biomaterials is very complex and influenced by many factors that have a direct or indirect

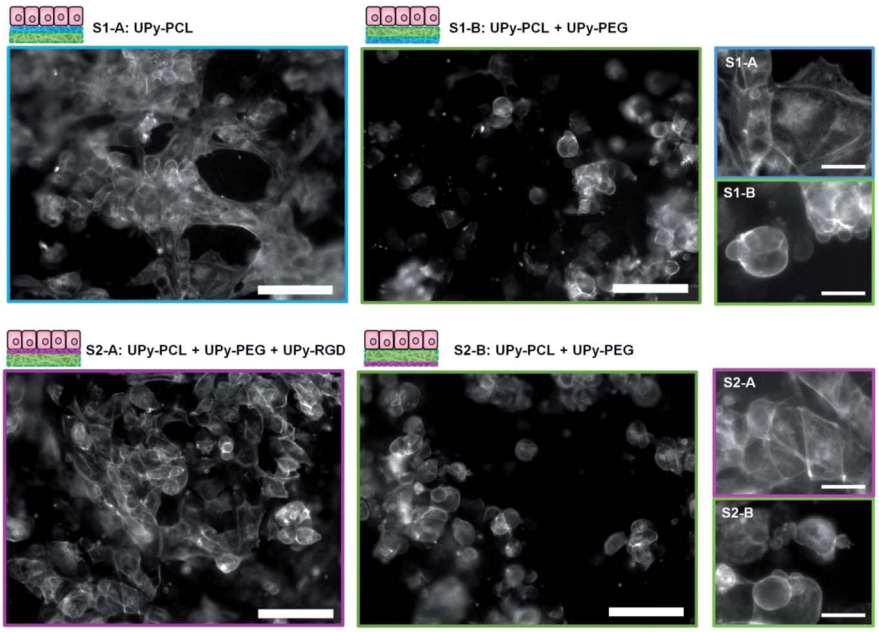


Fig. 4 Fluorescence microscopy images of HK-2 cells on the different bilayered scaffold sides 14 h after seeding. The actin cytoskeleton of the cells was stained and visualized. Scale bars represent 100 μm. In the enlarged views (right, scale bars represent 25 μm) the morphological differences between the HK-2 cells on the different scaffold sides are clearly seen. In the absence of UPy–PEG (S1-A) cells adhere and spread, in the presence of UPy–PEG (S1-B, S2-B) cells remain in a round morphology due to the lack of cell attachment. The presence of blebs in these cells indicates decoupling of the cytoskeleton from the plasma membrane and advancing apoptosis. Addition of UPy–RGD (S2-A) allows cells to adhere and spread, even in the presence of UPy–PEG.

effect. This complexity makes cell–biomaterial interaction studies rarely straightforward and often gives rise to varying results. As shown above, cells do adhere to some extent to the 'non-adhesive' scaffold sides, albeit cell morphology was observed to be less spread compared to the cell-adhesive scaffold sides. To investigate the cell–biomaterial interaction for our supramolecular UPy-based biomaterials in more detail, we seeded HK-2 cells on both dropcast films and electrospun meshes on glass. Both groups represented all three different UPy–biomaterial combinations that were used in the bilayered scaffolds. These samples allow for better fluorescence microscopy imaging (Fig. 5; $36 \times 10^3$ cells per sample seeded, referred to as a low cell density). For the different dropcast films a clear difference in the number of adhered cells and cell morphology is observed. Corresponding to what was observed for the bilayered scaffolds, fewer cells were adhered and spread on the non-cell adhesive combination (UPy–PCL + 30 wt% UPy–PEG), while the presence of UPy–RGD restores cell adhesion and spreading. Higher magnification images show that the lack of cell adhesion and spreading on the UPy–PCL + UPy–PEG dropcast film coincides with the lack of both a well-defined actin skeleton and vinculin rich focal adhesion points, which are formed by HK-2 cells cultured on the pure UPy–PCL and UPy–RGD supplemented films (Fig. 5a).

It is important to mention that for electrospun microfibrous substrates, the results are not always black and white. When HK-2 cells were seeded at a low density on electrospun meshes on glass (mesh morphologies are shown in the ESI, Fig. SI-5†), a comparable amount of cells seemed to adhere to all three UPy–biomaterial mixtures (Fig. 5b). When HK-2 cells were seeded at a higher density of $180 \times 10^3$ cells per sample, as was done for the bilayered scaffolds, more cells adhered, also on the presumed non-cell adhesive UPy–PCL + UPy–PEG mixture (ESI, Fig. SI-6†). This result is confirmed by the on average equal signal for the different UPy–biomaterial meshes in the resazurin assay (ESI, Fig. SI-8†). This assay measures the metabolic activity of the cells and as such is an indirect measure of the total amount of viable cells present on the meshes. Beside comparable cell numbers, the cell morphology appears to be similar for the different meshes at low magnification. For the UPy–PCL + UPy–PEG mixture this seems inconsistent with the distinctly rounded HK-2 cell morphology that was observed for bilayered scaffold sides S1-B and S2-B, which are of the same chemical composition. When cell–mesh interactions were studied in more detail differences between the different meshes were clearly visible. Higher magnification micrographs revealed vinculin rich focal adhesions which clearly co-locate with the fibers of the pure UPy–PCL. This was also visible for cells on the UPy–RGD containing mesh, although less pronounced due to the smaller electrospun microfiber diameters that are present in this mesh. Such focal adhesion formation was not observable 14 hours after cell seeding on the UPy–PCL + UPy–PEG mesh, showing the non-cell adhesive character of this UPy-polymer combination (Fig. 5b).

To investigate the development of these cultures in time, we also evaluated the low density cell cultures on electrospun meshes after 3 days. On all three different UPy–biomaterial compositions, the adhered cells proliferated and formed a

 

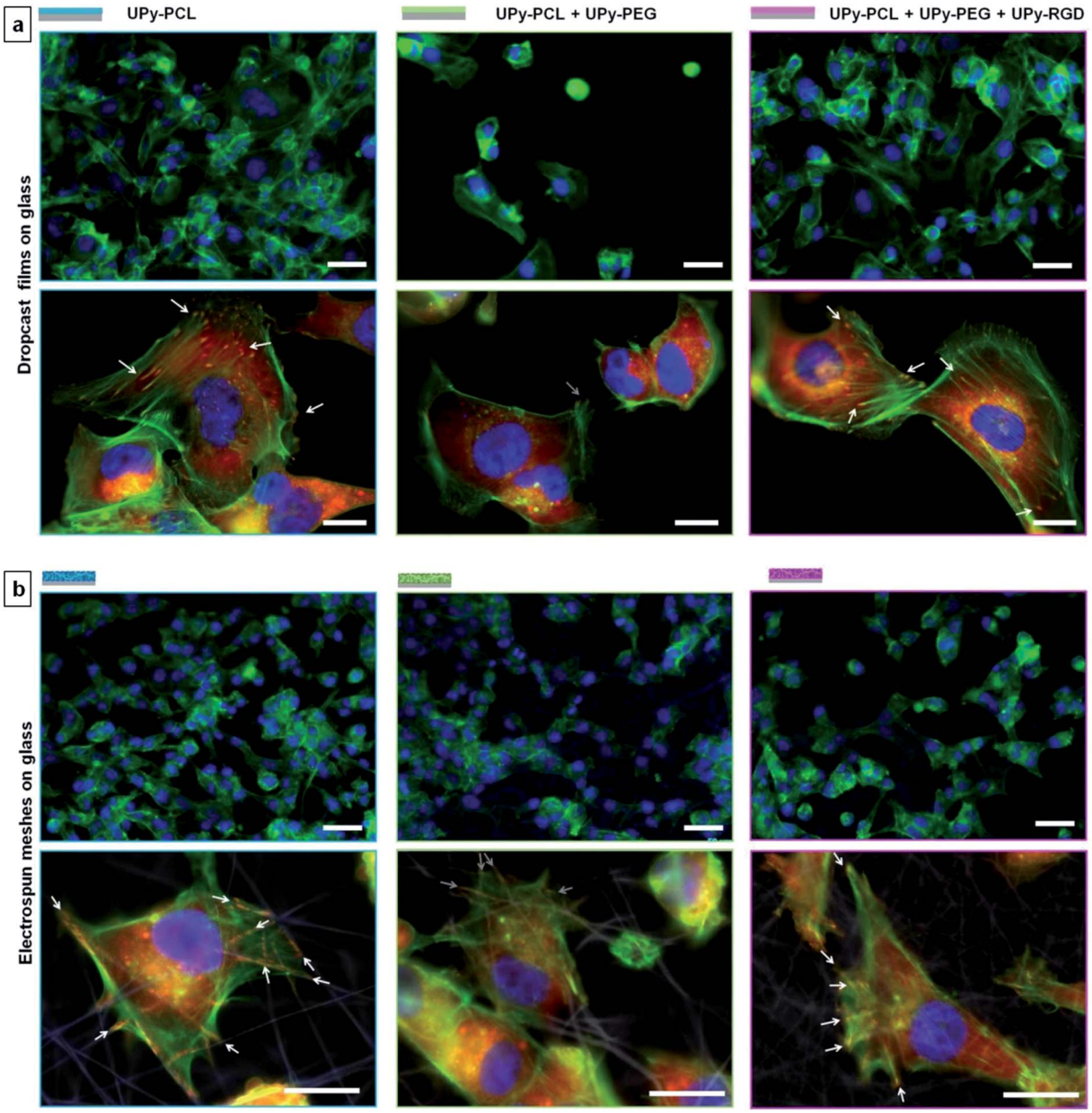


Fig. 5 Fluorescence micrographs of HK-2 cells, 14 h after seeding 36 × $10^3$ cells per sample, stained for actin (green), vinculin (red, for clarity not shown in the small magnification images) and cell nuclei (blue). (a) On pure UPy–PCL dropcast films HK-2 cells adhere and spread. In the presence of UPy–PEG fewer cells adhere and spread (relatively more cells remain in a round morphology due to the lack of proper cell attachment). The addition of UPy–RGD promotes cell adhesion (scale bars represent 50 μm). In the enlarged view (scale bars represent 20 μm) the morphological differences between the HK-2 cells on the different UPy-films are clearly visible. On UPy–PCL + UPy–PEG the cells display an ill-defined actin skeleton and vinculin is not concentrated in focal adhesion points. In the presence of UPy–RGD, vinculin-rich focal adhesion points are observed at the ends of well defined stress-fibers of the cytoskeleton, which is also seen for HK-2 cells seeded on pure UPy–PCL dropcast films (indicated by the white arrows). (b) For electrospun meshes, collected as thin layers of microfibers on a coverslip, the effect of UPy–PEG added to UPy–PCL on HK-2 cell adhesion is not clearly observed compared to the dropcast films (scale bars top row represent 50 μm). Hence, also no clear effect of UPy–RGD is seen. Higher magnification images show vinculin concentrated in focal adhesions, which co-locate with the electrospun fibers (indicated by white arrows, the arrow direction corresponds to the fiber direction, scale bars represent 20 μm). These focal adhesions are most pronounced for HK-2 cells adhered to an electrospun mesh consisting of pure UPy–PCL. On UPy–PCL + UPy–PEG focal adhesions are absent or not observed at places where they would be expected (indicated with gray arrows). In the presence of UPy–RGD the characteristic focal adhesion points are present (appear in yellow, due to overlap of red and green signals).

near-confluent cell layer with tight junction formation between the cells (ESI, Fig. SI-7†). Cell proliferation over time was confirmed by an increase of the total mitochondrial activity in the resazurin assay (ESI, Fig. SI-8†). Remarkably, when looking at a 3-day cell culture on bilayered scaffold side S1-B, the cells that initially adhered were not capable of such a development.

Instead of increasing cell numbers, fewer cells remained over time (ESI, Fig. SI-4†). Difference in cellular development on substrates with equal overall chemical composition is possible when deviations in surface distribution of the different building blocks are considered. Furthermore, it was recently shown that epithelial cells can form multicellular bridges over relatively long non-adherent areas,[46] thus spacing of adherent and non-adherent components can be crucial in determining whether epithelial cells can form a confluent monolayer or not.

These results underline not only the complexity of cell–biomaterial interactions in general, in which already many direct or indirect factors may play a role, but more specifically the difficulty when working with intrinsically dynamic supramolecular biomaterials. In comparison with covalently built-up biomaterials, supramolecular systems can adjust and change their properties in time and are more responsive towards their environment. This can be considered advantageous in combination with cells when the goal is to mimic natural cellular substrates. However, extra care has to be taken while interpreting experimental results when working with such materials.

Overall, we can conclude that the modular approach to make non-cell adhesive and reactivated cell-adhesive supramolecular substrates is possible using UPy–biomaterial building blocks. However, more work is needed to better understand which factors influence the 'supramolecular synthesis' of these materials, to gain in-depth insight in material dynamics, and to ultimately control the material and its dynamics, before total control over cell behavior can be established.

## Conclusions

In this paper we have demonstrated the use of a supramolecular approach to form anisotropic electrospun scaffolds, based on UPy-modified polymers and peptide building blocks. The advantage of this approach is that no covalent synthesis is needed to generate new biomaterials. Once the UPy-building blocks are available they can be mixed-and-matched to combine desired biomaterial properties. The effectiveness of this modular approach is demonstrated by the combination of up to three different UPy-building blocks in a single processing step. Properties attributed to the separate supramolecular building blocks such as mechanical stability, hydrophilicity, repulsion of cell-adhesion and induction of cell-adhesion are combined as desired by choosing and mixing the building blocks. By application of different mixtures in stepwise processing such as layered electrospinning, bilayered modular scaffolds with tailorable anisotropic properties are formed. However, additional research is needed to gain more control over building block distribution during 'supramolecular synthesis' of UPy–biomaterials, and with that further control over cellular behavior.

The choice of both polymer backbones and bioactive peptides that can be applied is endless. Therefore this UPy-based biomaterial system enables a combinatorial approach for the formation of new biomaterials. Combined with high throughput screening, *i.e.* a materiomics approach, this supramolecular biomaterial system is proposed to influence the exploration and identification of biomaterials with ECM-mimicking properties.

## Acknowledgements

The authors thank Eduard Ebberink and Bas Meusen for initial experiments, and Simone Hendrikse, Michel van Houtem and Henk Janssen for synthesis help. We thank Geert van Almen and Ewelina Burakowska-Meise for useful discussions. The research leading to these results has received funding from the Ministry of Education, Culture and Science (Gravity program 024.001.035), the Netherlands Organisation for Scientific Research (NWO), the European Research Council (FP7/2007-2013) ERC Grant Agreement 308045 and 246829, and from Marie Curie Actions (VLPsiRNA-FP7-PEOPLE-2009-IOF-254069 M.C.-A.). This research forms part of the Project P3.01 BioKid of the research program of the BioMedical Materials institute, co-funded by the Dutch Ministry of Economic Affairs. The financial contribution of the Dutch Kidney Foundation is gratefully acknowledged.

## References

1 L. Soletti, Y. Hong, J. Guan, J. J. Stankus, M. S. El-Kurdi, W. R. Wagner and D. A. Vorp, *Acta Biomater.*, 2010, **6**, 110–122.
2 J. S. Mao, L. G. Zhao, Y. J. Yin and K. D. Yao, *Biomaterials*, 2003, **24**, 1067–1074.
3 P. Nooeaid, J. A. Roether, E. Weber, D. W. Schubert and A. R. Boccaccini, *Adv. Eng. Mater.*, 2013, **15**, DOI: 10.1002/adem.201300072.
4 S. Kidoaki, I. K. Kwon and T. Matsuda, *Biomaterials*, 2005, **26**, 37–46.
5 M. P. Lutolf and J. A. Hubbell, *Nat. Biotechnol.*, 2005, **23**, 47–55.
6 B.-S. Kim and D. J. Mooney, *Trends Biotechnol.*, 1998, **16**, 224–230.
7 P. X. Ma and R. Zhang, *J. Biomed. Mater. Res.*, 1999, **46**, 60–72.
8 X. Wang, B. Ding and B. Li, *Mater. Today*, 2013, **16**, 229–241.
9 J. C. Adams and F. M. Watt, *Development*, 1993, **117**, 1183.
10 R. Timpl and J. C. Brown, *BioEssays*, 1996, **18**, 123–132.
11 E. Zamir and B. Geiger, *J. Cell Sci.*, 2001, **114**, 3583–3590.
12 J. de Boer and C. A. van Blitterswijk, *Materiomics: High-Throughput Screening of Biomaterial Properties*, Cambridge University Press, 2013.
13 A. L. Hook, D. G. Anderson, R. Langer, P. Williams, M. C. Davies and M. R. Alexander, *Biomaterials*, 2010, **31**, 187–198.
14 P. Y. W. Dankers and E. W. Meijer, *Bull. Chem. Soc. Jpn.*, 2007, **80**, 2047–2073.
15 J.-M. Lehn, *Chem. Soc. Rev.*, 2007, **36**, 151–160.
16 C. Viney, *Mater. Sci. Rep.*, 1993, **10**, 187–236.
17 H. Cui, M. J. Webber and S. I. Stupp, *Pept. Sci.*, 2010, **94**, 1–18.
18 J. H. Collier, J. S. Rudra, J. Z. Gasiorowski and J. P. Jung, *Chem. Soc. Rev.*, 2010, **39**, 3413–3424.

 

19 P. H. J. Kouwer, M. Koepf, V. A. A. Le Sage, M. Jaspers, A. M. van Buul, Z. H. Eksteen-Akeroyd, T. Woltinge, E. Schwartz, H. J. Kitto, R. Hoogenboom, S. J. Picken, R. J. M. Nolte, E. Mendes and A. E. Rowan, *Nature*, 2013, **493**, 651–655.
20 S. MacNeil, *Mater. Today*, 2008, **11**, 26–35.
21 S. Korossis, F. Bolland, E. Ingham, J. Fisher, J. Kearney and J. Southgate, *Tissue Eng.*, 2006, **12**, 635–644.
22 A. Mangera, A. J. Bullock, C. R. Chapple and S. MacNeil, *Neurourol. Urodyn.*, 2012, **31**, 13–21.
23 A. Mol, A. I. P. M. Smits, C. V. C. Bouten and F. P. T. Baaijens, *Expert Rev. Med. Devices*, 2009, **6**, 259–275.
24 P. Aebischer, T. K. Ip, G. Panol and P. M. Galletti, *Life Support Syst.*, 1987, **5**, 159–168.
25 H. D. Humes, *Semin. Nephrol.*, 2000, **20**, 71–82.
26 A. Saito, K. Sawada and S. Fujimura, *Hemodialysis International*, 2011, **15**, 183–192.
27 H. Zhang, F. Tasnim, J. Y. Ying and D. Zink, *Biomaterials*, 2009, **30**, 2899–2911.
28 M. Ni, J. Teo, M. S. Ibrahim, K. Zhang, F. Tasnim, P. Y. Chow, D. Zink and J. Y. Ying, *Biomaterials*, 2011, **32**, 1465–1476.
29 H. Ueda, J. Watanabe, T. Konno, M. Takai, A. Saito and K. Ishihara, *J. Biomed. Mater. Res., Part A*, 2006, **77A**, 19–27.
30 W. Halfter, C. Monnier, D. Müller, P. Oertle, G. Uechi, M. Balasubramani, F. Safi, R. Lim, M. Loparic and P. B. Henrich, *PLoS One*, 2013, **8**, e67660.
31 F. H. Beijer, R. P. Sijbesma, H. Kooijman, A. L. Spek and E. W. Meijer, *J. Am. Chem. Soc.*, 1998, **120**, 6761–6769.
32 H. Kautz, D. J. M. van Beek, R. P. Sijbesma and E. W. Meijer, *Macromolecules*, 2006, **39**, 4265–4267.
33 R. P. Sijbesma, F. H. Beijer, L. Brunsveld, B. J. B. Folmer, J. H. K. K. Hirschberg, R. F. M. Lange, J. K. L. Lowe and E. W. Meijer, *Science*, 1997, **278**, 1601–1604.
34 P. Y. W. Dankers, J. M. Boomker, A. H. der Vlag, F. M. M. Smedts, M. C. Harmsen and M. J. A. van Luyn, *Macromol. Biosci.*, 2010, **10**, 1345–1354.
35 P. Y. W. Dankers, J. M. Boomker, A. Huizinga-van der Vlag, E. Wisse, W. P. J. Appel, F. M. M. Smedts, M. C. Harmsen, A. W. Bosman, E. W. Meijer and M. J. A. Luyn, *Biomaterials*, 2011, **32**, 723–733.
36 R. E. Kieltyka, M. M. C. Bastings, G. C. van Almen, P. Besenius, E. W. L. Kemps and P. Y. W. Dankers, *Chem. Commun.*, 2012, **48**, 1452–1454.
37 P. Y. W. Dankers, M. C. Harmsen, L. A. Brouwer, M. J. A. Van Luyn and E. W. Meijer, *Nat. Mater.*, 2005, **4**, 568–574.
38 E. Wisse, A. J. H. Spiering, P. Y. W. Dankers, B. Mezari, P. C. M. M. Magusin and E. W. Meijer, *J. Polym. Sci., Part A: Polym. Chem.*, 2011, **49**, 1764–1771.
39 M. C. Lensen, V. A. Schulte and M. Diez, in *Biomaterials – Physics and Chemistry*, ed. R. Pignatello, InTech, 2011.
40 U. Hersel, C. Dahmen and H. Kessler, *Biomaterials*, 2003, **24**, 4385–4415.
41 P. Y. W. Dankers, PhD thesis, Eindhoven University of Technology, 2006.
42 P. Y. W. Dankers, P. J. H. M. Adams, D. W. P. M. Löwik, J. C. M. van Hest and E. W. Meijer, *Eur. J. Org. Chem.*, 2007, 3622–3632.
43 M. J. Ryan, G. Johnson, J. Kirk, S. M. Fuerstenberg, R. A. Zager and B. Torok-Storb, *Kidney Int.*, 1994, **45**, 48–57.
44 F. Ahmed, N. R. Choudhury, N. K. Dutta, A. Zannettino and R. Knott, *Biomacromolecules*, 2013, **14**, 3850–3860.
45 A. Polini, S. Pagliara, R. Stabile, G. S. Netti, L. Roca, C. Prattichizzo, L. Gesualdo, R. Cingolani and D. Pisignano, *Soft Matter*, 2010, **6**, 1668–1674.
46 S. R. K. Vedula, H. Hirata, M. H. Nai, A. Brugués, Y. Toyama, X. Trepat, C. T. Lim and B. Ladoux, *Nat. Mater.*, 2014, **13**, 87–96.